

Application of Nickel Ferrite Nanoparticles in Adsorption of Amoxicillin Antibiotic

Patricia M. A. Caetano,^{✉*,a,b,c} Nathália M. Simões,^a Paula S. Pinto,^{c,d}
Luis E. Fernandez-Outon,^{a,e} Adriana S. Albuquerque,^a Waldemar A. A. Macedo^a
and José D. Ardisson^a

^aCentro de Desenvolvimento da Tecnologia Nuclear (CDTN), Av. Presidente Antônio Carlos, 6627,
31270-901 Belo Horizonte-MG, Brazil

^bCentro Universitário UNA, Rua dos Aimorés, 1451, 30140-071 Belo Horizonte-MG, Brazil

^cDepartamento de Química, Universidade do Estado de Minas Gerais (UEMG),
35501-170 Divinópolis-MG, Brazil

^dDepartamento de Química, Universidade Federal de Minas Gerais (UFMG),
31270-901 Belo Horizonte-MG, Brazil

^eDepartamento de Física, Universidade Federal de Minas Gerais (UFMG),
31270-901 Belo Horizonte-MG, Brazil

According to the World Health Organization, amoxicillin (AMX) is the most widely consumed antibiotic in the world. Consequently, there is great interest in the development of new technologies that allow the removal of this type of contaminant, as exposure to antibiotic residues can cause a variety of adverse effects, such as toxicity and antimicrobial resistance. In this work, AMX adsorption from aqueous solution was investigated using nickel ferrite nanoparticles. The nanoadsorbents were prepared by the coprecipitation method, annealed at 300 to 700 °C, and characterized by X-ray diffraction (XRD), transmission electron microscopy (TEM), Mössbauer spectroscopy (ME) and vibratory sample magnetometry (VSM). Nanoparticle size, pH and temperature were found to significantly affect the amount of adsorbed AMX. The pseudo-second order kinetic model described the adsorption process and the adsorption isotherm fitted to the Freundlich model. AMX adsorption capacity was 104–45 mg g⁻¹ (milligram of AMX per gram of ferrite) for ferrite annealed at 300–700 °C, respectively. The nanoadsorbents employed showed higher AMX removal efficiency when compared to other iron oxides. Moreover, the good reuse results obtained showed their great potential for antibiotic removal by adsorption.

Keywords: ferrite, adsorption, amoxicillin, beta-lactam

Introduction

Water quality is one of the major environmental concerns today. In particular, the occurrence and destination of drugs to the aquatic environment in recent decades has been recognized as one of the emerging problems of our civilization, since they affect both the Earth's ecosystems, and the health and quality of life of the human beings.¹ According to World Health Organization report² on surveillance of antibiotic consumption, amoxicillin (AMX) is the most widely used antibiotic in the world. Furthermore, this antibiotic presents significant ecotoxicity, as suggested

by several ecological risk studies^{3,4} for the environment, and also creates drug resistance. Consequently, it is of paramount interest the development of new technologies that allow the effective removal of this type of contaminant from aqueous matrices.^{2,5,6}

Conventional water treatment systems do not guarantee the removal of a number of micropollutants, especially drugs. Different studies including photocatalysis,⁷ biodegradation,⁸ nanofiltration,⁹ thermal treatment¹⁰ and adsorption^{4,6} have been applied in drug removal processes. However, of all treatment methods that have been developed, adsorption is the most effective and promising method for removing organic and inorganic micro pollutants, due to their low cost, reproducibility,

*e-mail: patriciamacaetano@gmail.com

simple operation, and effectiveness.¹¹ The choice of adsorbent with exceptional adsorption efficiency is key to the adsorption technique. Carbon nanotubes and activated carbon have been studied to promote amoxicillin adsorption, but there are some limitations on the use of these materials as adsorbent. Adsorption using activated carbon is relatively expensive because activated carbon is hardly regenerated after adsorption, and microporous activated carbon, although efficient, has a limitation in the adsorption process due to the relatively large size of AMX molecules. When evaluating carbon nanotubes, these materials are very hydrophobic and poor interaction with water makes the adsorption process difficult.¹²⁻¹⁴

Among the new generation of adsorbent materials, magnetic nanoadsorbents are the most promising, due to the different properties such as: high surface area, adjustable morphology, and high efficiency, being easily separated from the solution after the adsorption process.¹⁵

In this context, ferrite nanoparticles have shown interesting properties as adsorbents in the removal of AMX in aqueous solutions.¹⁶ The most relevant characteristics in the adsorptive capacity of NiFe₂O₄ nanoparticles include: increased specific surface area and high adsorption capacity; besides, the ferrite spinel geometry consists of two types of sites, tetrahedral sites (A) and octahedral sites (B), which play a significant role in the control of the adsorption characteristics and magnetic properties.^{17,18} The superparamagnetic behavior allows easy separation from liquids/solids and eventually the regeneration and recycling of magnetic adsorbents. In addition, it is known that iron and other transition metals such as Co²⁺, Co³⁺ and Ni²⁺ can complex with antibiotic molecules.¹⁹ Although the publications in the area of environmental remediation are increasing in the last years, by the time of preparation of this article it has not been found any published article specifically related to the capacity of adsorption of amoxicillin by NiFe₂O₄ nanoparticles synthesized by coprecipitation method and annealed at different temperatures.

In this work, the adsorption and subsequent removal of AMX from aqueous solution was investigated using NiFe₂O₄ nanoparticles annealed at temperatures ranging from 300 to 700 °C. Samples were prepared by the coprecipitation method and characterized by X-ray diffraction (XRD), Mössbauer spectroscopy (MS), transmission electron microscopy (TEM), vibrating sample magnetometry (VSM) and the specific surface area was determined by Brunauer-Emmet-Teller (BET) method based on adsorption/desorption isotherms of nitrogen. The effects of different operational parameters that affect the removal process were investigated: adsorbent amounts, contact time, temperature and surface area.

Experimental

NiFe₂O₄ nanoparticles were prepared by chemical coprecipitation method. Aqueous solution of iron nitrate [(Fe(NO₃)₃·9H₂O)] (Dinâmica, São Paulo, SP, Brazil) and nickel nitrate [(Ni(NO₃)₂·6H₂O)] (Dinâmica, São Paulo, SP, Brazil), with stoichiometric ratio Ni:Fe = 1:2 were stirred for 1 h (for each 1 g of nitrate, 3.3 mL of Milli-Q water (Millipore, Bedford, USA) were used). After this period, the nitrates were added to the NaOH (Neon, Suzano, SP, Brazil). It was used 3.3 g of NaOH diluted in 31.0 mL for each 1 g of nitrate, followed by further stirring for 15 min. The resultant materials were annealed at different temperatures in a muffle furnace for a period of 2 h, in ordinary atmosphere.^{20,21} The annealing temperatures used were 300, 400, 500, 600 and 700 °C to obtain different particles sizes. The particle size, morphology, specific surface area and magnetic properties of the adsorbent NiFe₂O₄ nanoparticles were measured using XRD, TEM, MS and VSM. The specific surface area was determined by BET method based on adsorption/desorption isotherms of nitrogen. The zeta potential has been measured with a Malvern NanoZS HT Zetasizer. The analyses were performed with a concentration of 0.5 mg mL⁻¹ of the samples of ferrites dispersed in Milli-Q water, the pH variation was performed using 0.5 mol L⁻¹ sodium hydroxide (Neon, Suzano, SP, Brazil) and 0.5 mol L⁻¹ hydrochloric acid (Neon, Suzano, SP, Brazil).

The adsorption experiments were performed using 20 mL of AMX solution with a concentration of 200 mg L⁻¹ and 20 mg of ferrite, at pH 7. The mixture was stirred at 200 rpm for 24 h at 25 °C, filtered using a 45 µm syringe filter, and analyzed on a spectrophotometer (T60 UV-Visible, PG Instruments). The AMX removal was calculated using the adsorption band at 272 nm (see Figure S1, Supplementary Information (SI) section).¹³ The adsorbed quantity *per* unit mass of ferrite and the percentages of adsorbates removed were calculated using equations 1 and 2, respectively.

$$q = \frac{(c_o - c_f)V}{m} \quad (1)$$

$$\text{Removal}(\%) = \frac{(c_o - c_f)}{c_o} \times 100 \quad (2)$$

where, *q* is amount of adsorbed AMX *per* gram of ferrite (mg g⁻¹), *C_o* and *C_f* are the concentration of AMX at the initial time (*t* = 0) and after a given time (*t*) (mg L⁻¹), respectively, *V* is the volume of the aqueous phase (L) and *m* is the mass of the adsorbent (g).

The effects of pH (2-11), contact time (0-2880 min), initial AMX concentration (25-250 mg L⁻¹) and temperature (20-40 °C) of the AMX solution were investigated. Also, kinetics and adsorption isotherms were analyzed. Competitive adsorption experiments were carried out using 200 mg L⁻¹ AMX solutions in the presence of phosphate. The capacity of reuse of NiFe₂O₄ in the adsorption of AMX was evaluated. After the first use, the nanoparticles were recovered by magnetic separation. Using a filter to retain the adsorbent, nanoparticles were washed with Milli-Q water to remove the AMX adsorbed on their surface and then dried. Subsequently, the material was used again under the same experimental conditions mentioned previously.

Results and Discussion

XRD spectra of NiFe₂O₄ samples annealed at 300, 400, 500, 600 and 700 °C are shown in Figure 1. All the reflection planes observed in the diffractograms confirmed the formation of the cubic spinel structure of nickel ferrite (reference data of Joint Committee on Powder Diffraction Standards, JCPDS card No. 742081). A significant increase in intensity and reduction of the width of the diffraction peaks was observed, indicating an increase in crystallinity and particle diameter with increasing annealing temperature. These results agree with published data²² for Co and Ni ferrite

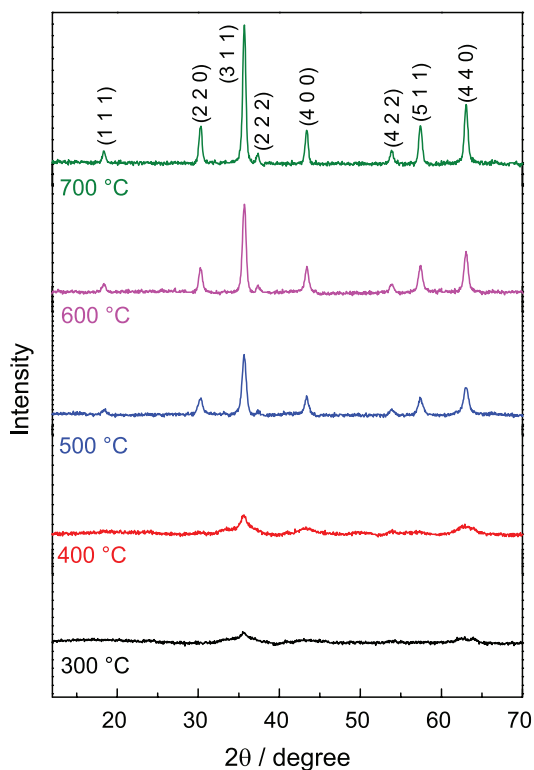


Figure 1. XRD patterns of NiFe₂O₄ nanoparticles annealed at different temperatures.

Table 1. Average particle size, specific area and pore volume of NiFe₂O₄ samples

Annealing temperature / °C	Mean crystallite size / nm	Specific surface area / (m ² g ⁻¹)	Total pore volume / (cm ³ g ⁻¹)
300	4 ± 2	212	0.23
400	6 ± 2	147	0.25
500	16 ± 2	53	0.20
600	20 ± 2	31	0.16

nanoparticles. The mean particle diameter estimated by the Scherrer equation ranged from 3 to 25 nm (Table 1).

The shape, size and morphology of the single-phase particles were examined by direct observation (TEM). The TEM micrographs corresponding to the sample annealed at 400 °C, shown in Figure 2, reveal that the particles are approximately spherical, with median diameter of 10 nm and standard deviation of 3 nm.

The surface area of the ferrites was measured using nitrogen adsorption/desorption isotherms at 77 K by the BET method (Table 1). Samples annealed at 300 °C have higher surface area compared to the other samples. This result was already expected since the increase of the annealing temperature favors particle growth, as verified by XRD, and consequently the surface area is reduced. The values obtained are similar to those found in the literature.^{23,24}

Figure 3a shows the adsorption and desorption isotherms of N₂, in addition to the pore diameter distribution curve. The samples showed isothermal profiles characteristic of mesoporous materials (type IV according to the International Union of Pure and Applied Chemistry, IUPAC, classification).²⁵ The pore diameter distribution profiles, shown in Figure 3b, exhibit a narrow range of pore distribution, in which the majority of the pore diameter is located in the 2 to 20 nm range, characteristic of mesoporous materials.²⁵

Mössbauer spectra were measured at 25 and at -248.5 °C (Figure 4). The spectra were fitted using sextets, associated to Fe³⁺ in tetrahedral (A) and octahedral (B) sites. Samples annealed at 300 and 400 °C exhibit collapsed hyperfine fields at (A) and (B) sites, suggesting superparamagnetic behavior at room temperature. Spectra for samples annealed at 500, 600 and 700 °C exhibit narrower lines, due to an increased degree of crystallinity.²⁶ The hyperfine parameters obtained from the fitting of the spectra are shown in Table 2.

The M-H hysteresis loops were measured using a vibrating sample magnetometer (Figure 5). It is observed that the saturation magnetization (M_S) increases with

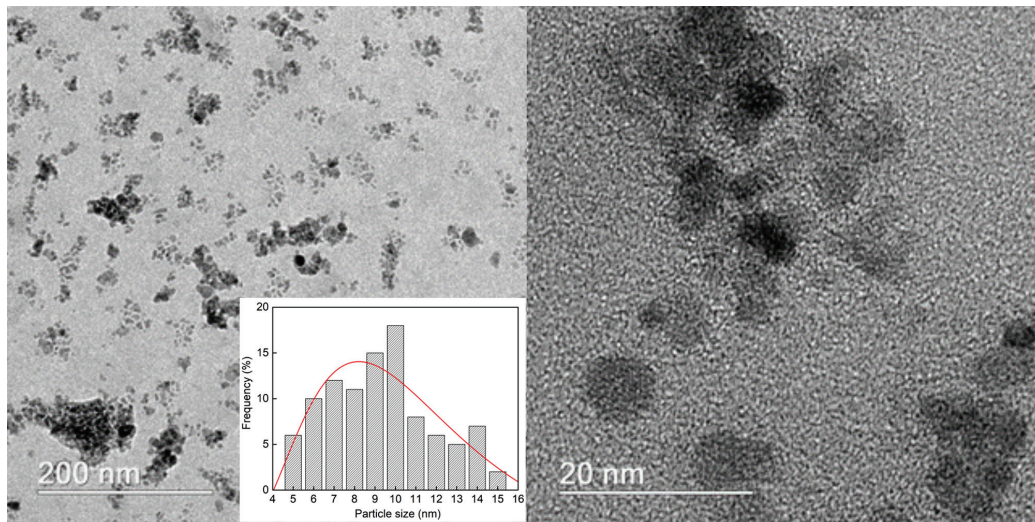


Figure 2. TEM images of NiFe_2O_4 annealed at 400 °C.

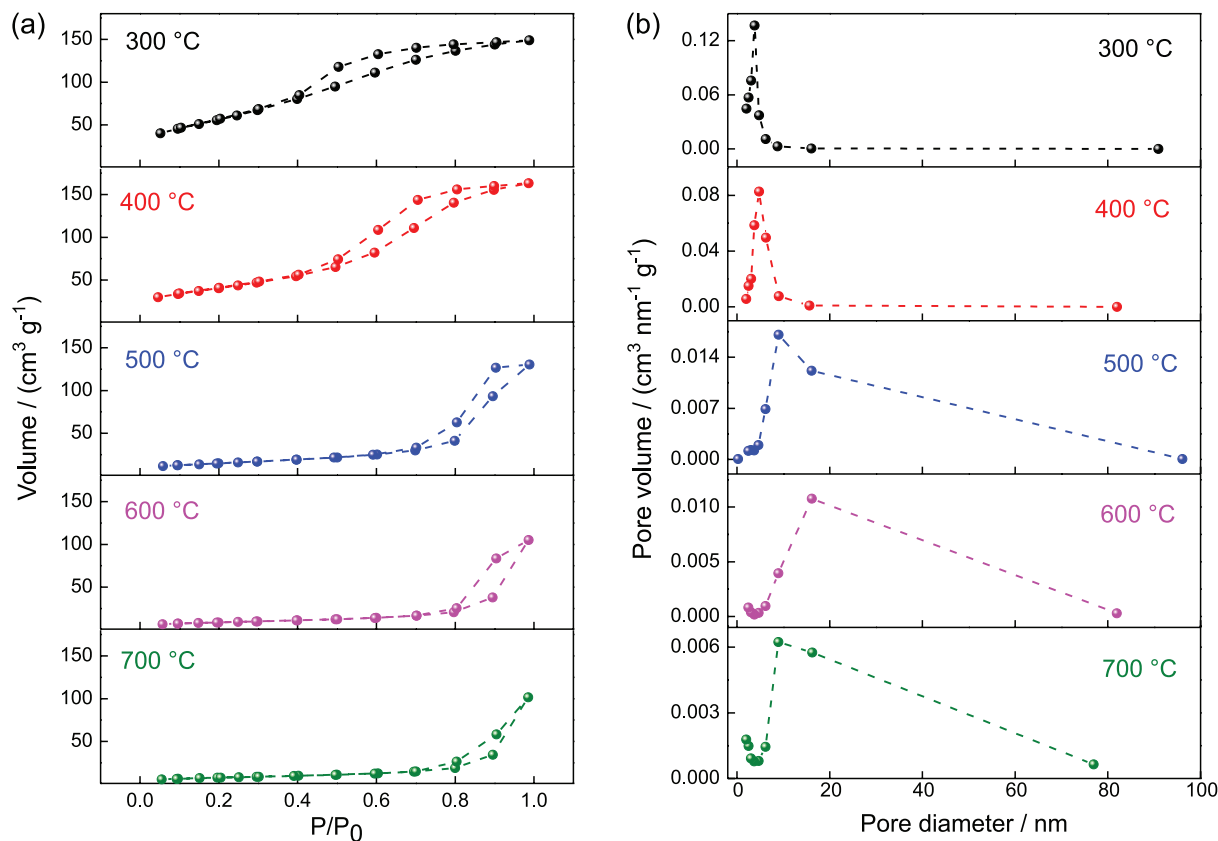


Figure 3. (a) N_2 adsorption-desorption isotherms and (b) pore size distribution curves of NiFe_2O_4 annealed at 300, 400, 500, 600 and 700 °C.

annealing temperature, as consequence of the particle size increase, which involves the reduction of surface to volume spins, and consequently resulting in the enhancement of saturation magnetization. Table 2 shows the variation of coercivity (H_C) with annealing temperature, being largest for the nanoparticles annealed at 600 °C, having mean diameter of 20 nm. It is well known that H_C is very sensitive

to the particle size distribution. It is observed that up to 600 °C both particle size and coercivity increase. However, for annealing temperatures above 600 °C, the coercivity decreases, even though the particle size is still larger.²⁷ This fact should be related to a transition from monodomain to multidomain around these values of the particle diameter or a change in the magnetization reversal mode.²⁸

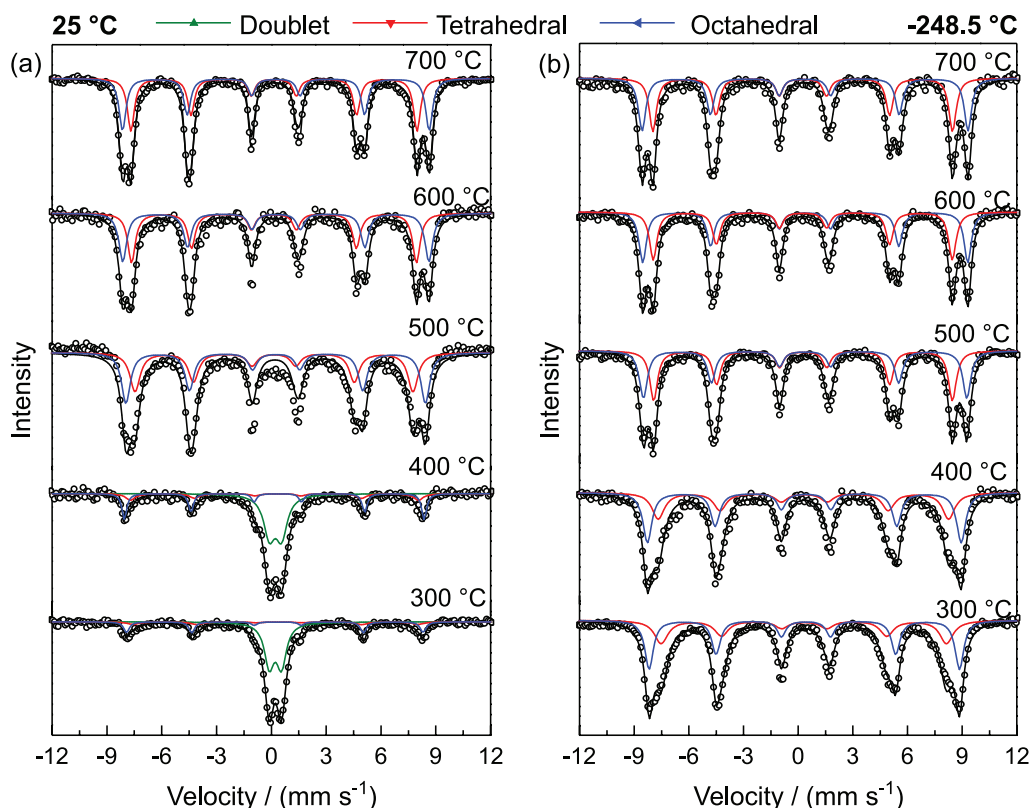


Figure 4. Mössbauer spectra for NiFe_2O_4 annealed at different temperatures measured at (a) 25 and (b) -248.5 °C.

Table 2. Hyperfine parameters, saturation magnetization and coercivity of NiFe_2O_4 samples

T / °C	Site	$\delta \pm 0.05$ / (mm s^{-1})		$\epsilon \pm 0.05$ / (mm s^{-1})		$B_{\text{HF}} \pm 0.5$ / T		RA ± 1 / %		$M_s \pm 3$ / (emu g^{-1})	$H_c \pm 3$ / Oe		
		Mössbauer spectroscopy measurement temperature / °C											
		25	-248.5	25	-248.5	25	-248.5	25	-248.5				
300	sextet A	0.32	0.32	-0.19	-0.02	48	48	9	37	8	11		
	sextet B	0.33	0.38	-0.15	-0.09	50	52	21	63				
	doublet	0.22		0.67		-		70					
400	sextet A	0.25	0.31	-0.19	-0.03	48	49	8	40	9	19		
	sextet B	0.27	0.38	-0.20	-0.09	50	53	27	60				
	doublet	0.22		0.66		-		65					
500	sextet A	0.14	0.27	0.01	-0.01	47	50	42	46	32	45		
	sextet B	0.25	0.38	-0.03	0.00	50	55	58	54				
600	sextet A	0.14	0.26	0.01	-0.01	48	50	47	48	36	110		
	sextet B	0.25	0.37	-0.02	0.02	51	55	53	52				
700	sextet A	0.14	0.25	0.01	-0.01	48	51	48	49	39	45		
	sextet B	0.25	0.37	-0.01	-0.02	52	55	52	51				

T: annealing temperature; δ : isomer shift relative to α -Fe at room temperature; ϵ : quadrupole splitting; B_{HF} : hyperfine field; RA: relative spectral areas; M_s : saturation magnetization; H_c : coercivity.

Nanoparticles of nickel ferrite annealed at 300, 400, 500, 600 and 700 °C were subjected to AMX adsorption experiments, and the results are shown in Figure 6a. It was observed that increasing the annealing temperature caused a reduction in the adsorption capacity of the samples, as

expected, since the adsorption is a surface phenomenon, and, therefore, materials with greater surface area have greater capacity of adsorption.²⁹

High surface area and especially mesoporosity are important for the entry of the relatively large molecules

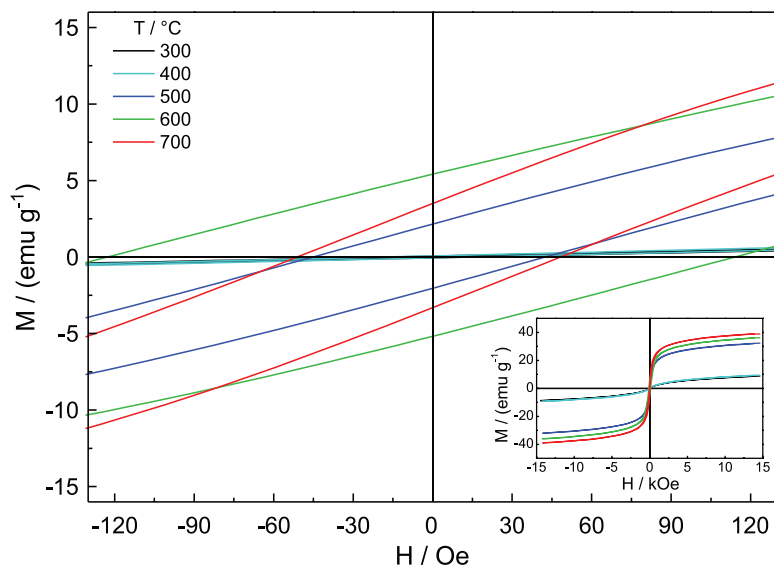


Figure 5. Hysteresis loops of NiFe₂O₄ annealed at different temperatures.

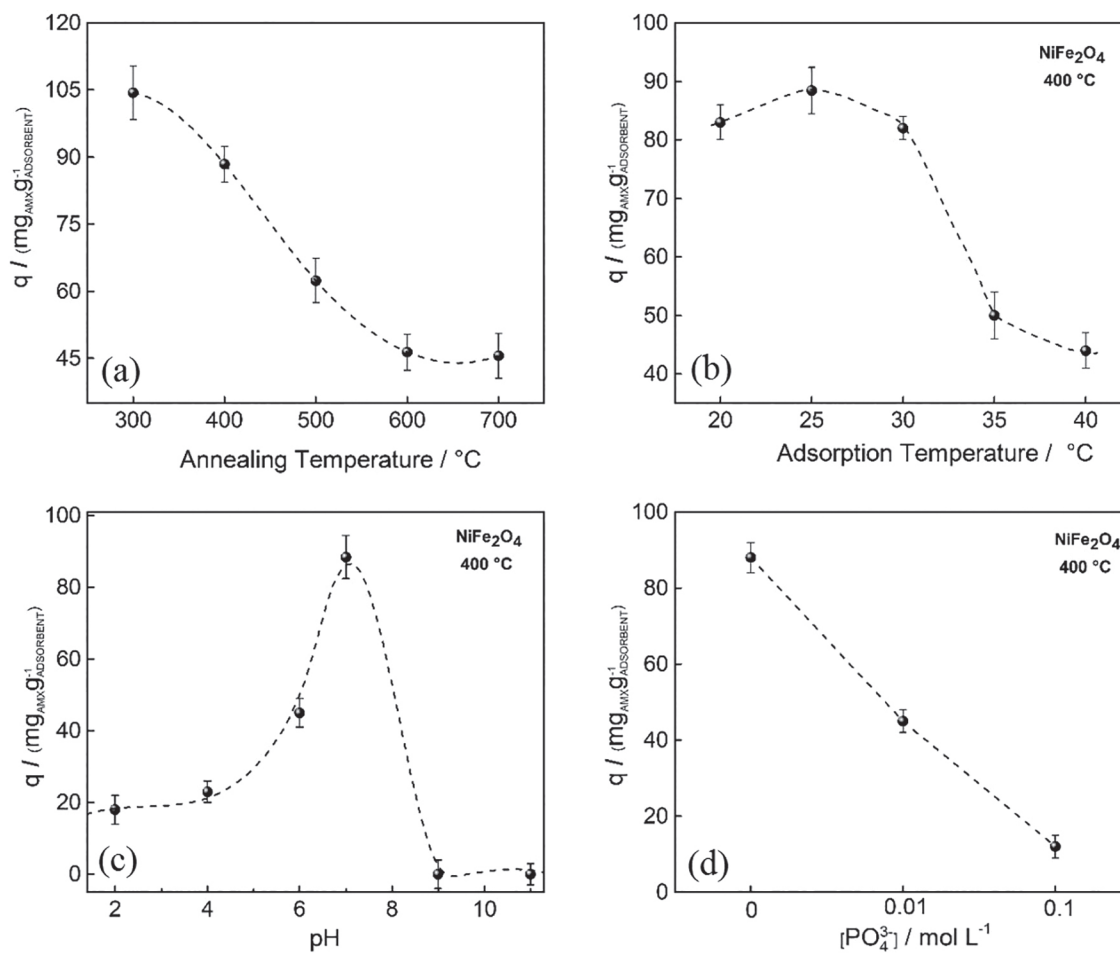


Figure 6. (a) Adsorptive capacity in the removal of amoxicillin from nickel ferrite nanoparticles annealed at different temperatures per gram of ferrite; effect of (b) temperature, (c) pH on the adsorption process of amoxicillin and (d) amoxicillin adsorption in the presence of phosphate.

of antibiotics to interact with the specific sites on the surface of the adsorbent.¹³ However, despite the surface area is important for increased adsorption rates, there

are other factors playing a major role in the adsorption process. Previous works^{5,13,30-32} indicate that iron and nickel species can interact with beta-lactam antibiotics through a

complexation, forming stable intermediates and allowing increased adsorption of AMX. Those transition metals show variable oxidation states according to the catalyst, reacting element or compound, and the conditions of the reaction in which they are involved. Thus, they can form a large number of complex compounds.³³

The NiFe₂O₄ ferrite at 400 °C was chosen as the model for more specific tests, such as temperature and pH, influence on adsorption, equilibrium isotherms and adsorption kinetics. Although this sample did not present the best adsorptive capacity compared to the annealed sample at 300 °C, it was selected because of its better crystallinity and its more pronounced magnetic properties, facilitating its removal in dispersion.

The effect of the solution temperature on the adsorption process was studied between 20 and 40 °C, using NiFe₂O₄ annealed at 400 °C. The results obtained are shown in Figure 6b. It can be observed that between 20 and 30 °C, the temperature does not significantly influence the adsorption process. However, at 35 and 40 °C there is a marked decrease on the adsorption rate. Equilibrium and kinetic studies of adsorption in aqueous solution indicate that this effect may be related to the weakening of the ligand forces between the active sites of the adsorbent and the adsorbate molecules.³⁴

The pH is one of the most important factors that could affect the adsorption process of organic materials, since the solubility of adsorbate and electric charge of the active sites on material surface can change depending on the pH value.^{35,36} In order to evaluate the pH effect of the solution in the adsorption process, experiments varying the pH from 2 to 11 were performed (Figure 6c). The amount of amoxicillin adsorbed increased in the range of pH 2 to 7 and the best result for amoxicillin removal was at pH 7, corresponding to 87 mg_{AMX} g_{ADSORBENT}⁻¹.

Amoxicillin is an amphoteric compound, thus presents more than one dissociation constants. The relationship between the pH effect of the solution and the adsorption of amoxicillin by the ferrite nanoparticles can be explained by considering the surface charge of the adsorbent and the dissociation constant (pK_a).^{37,38} At this point, it is interesting to consider that nickel ferrites annealed at 400 °C have point of zero charge (PZC) around 7.7 (see Figure S2, SI section) meaning that its surface is positively charged. AMX has three dissociation constants (pK_{a1} = 2.68, pK_{a2} = 7.49 and pK_{a3} = 9.63) and is mainly in the zwitterion form at pH values between 3 and 7. There is a β-lactam ring in its structure, making it susceptible to degradation by acid or basic hydrolysis.³⁹ Therefore, it is expected that in extreme pH values the degradation of AMX will occur.

Besides the adsorptive capacity, the leaching of the metals is another factor that depends on the pH value, and

in more acidic pHs there is an increase of the solubility of the metal in solution.⁴⁰ Atomic absorption measurements in the aqueous phase showed no significant Fe³⁺ leaching from the material. The highest values found were in pH 2 and 4, of 1.3 and 0.2 ppm of Fe³⁺, respectively.

The study of the equilibrium adsorption is of great importance for the understanding of the mechanisms that govern the interactions of a molecule with a solid sorbent.⁴¹ For this purpose, the Langmuir and Freundlich isotherm models were used to fit the experimental data.⁴² The results are summarized in Table 3 and Figure 7a.

Table 3. Parameters of the Langmuir and Freundlich isotherms

	Langmuir		Freundlich
q / (mg g ⁻¹)	97.654 ± 0.040	K	1.177 ± 0.090
b	0.054 ± 0.080	n	1.393 ± 0.021
R ²	0.446	R ²	0.993

q: amount of solute adsorbed *per* gram of adsorbent; b: constant equilibrium; K: experimental constant, which indicates the adsorption capacity of the adsorbent; n: experimental constant, which indicates the effect of concentration on adsorption capacity; R²: coefficient of determination.

Experimental data were best fitted by a Freundlich isotherm, using equation 3, where K_F and n are the Freundlich constants associated to relative capacity and to the adsorption intensity, respectively, C_e is the equilibrium concentration, and q_e is the amount of adsorbate adsorbed.

$$\log q_e = \ln K_F + \frac{1}{n} \log C_e \quad (3)$$

These results indicate that the adsorbent material is expected to have a heterogeneous surface, where the adsorption occurs in multilayers, having active sites with different energies.^{43,44}

Figure 7b shows the contact time required to reach equilibrium of AMX adsorption. It is observed that initially the adsorption process is very fast, decreasing gradually until equilibrium is reached, after 10 h. The adsorption kinetics of AMX was studied using pseudo-first and pseudo-second order models.⁴⁵ The calculated values of K (experimental constant) and q_e are shown in Table 4. Comparison of the coefficient of determination (R²) values obtained from the fittings indicates that the second-order model was the best suited to the experimental data (Figure 7b). The pseudo-second order kinetic model may be represented as:

$$\frac{1}{q_t} = \frac{1}{K_2 q_e^2} + \frac{t}{q_e} \quad (4)$$

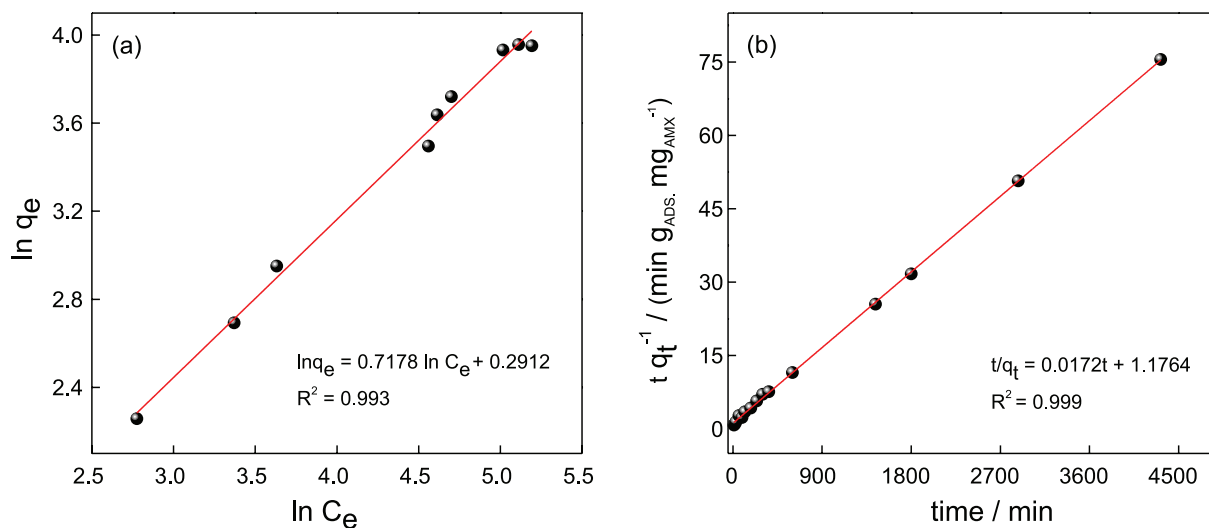


Figure 7. Linearization of (a) adsorption isotherm using the Freundlich model and (b) kinetic curve using the pseudo-second order model.

where K_2 is the second-order rate constant and q_t is the adsorption capacity of the adsorbent at time t . The values of t/q_t are plotted against t , q_e and K_2 are calculated from the slope and intercept of the plot. The second-order model considers the adsorption process as a chemical reaction, chemisorption.⁴⁶ Thus, it can be said that the rate of AMX adsorption by NiFe_2O_4 nanoparticles is controlled by chemisorption routes, which would involve ion exchange by means of valence forces through the exchange or share of electrons between adsorbate and adsorbent.⁴⁵

Table 4. Parameters of the kinetic models of pseudo-first and pseudo-second order

	Pseudo-first order		Pseudo-second order
$q_e / (\text{mg g}^{-1})$	15.31 ± 0.01	$q_e / (\text{mg g}^{-1})$	69.20 ± 0.01
$K_1 / (\text{g mg}^{-1} \text{min}^{-1})$	0.50 ± 0.01	$K_2 / (\text{g mg}^{-1} \text{min}^{-1})$	0.85 ± 0.01
R^2	0.729	R^2	0.999

q_e : amount adsorbed at equilibrium time; K_1 and K_2 : experimental constants; R^2 : coefficient of determination.

Aiming to understand the adsorption mechanisms, mainly related to the interaction of iron with the AMX molecule, a competitive adsorption experiment was carried out using phosphates. There is an expressive interaction of the phosphate anions with iron oxides, so the presence of phosphate competes with the complexation of other organic binders.^{47,48} Experiments were performed varying the phosphate concentration to evaluate the effect on the AMX adsorption (Figure 6d).

In absence of phosphate the adsorption of AMX was 88 mg g^{-1} and in presence of phosphate anions, adsorption capacity decreased to 12 mg g^{-1} at the same concentration (200 mg L^{-1}) of AMX. This sharp decrease in adsorption

capacity with increasing phosphate concentration provides evidence of the remarkable affinity of iron for this anion. Therefore, the strong affinity of phosphates to bind to iron species hampers the interaction between AMX and the Fe^{3+} species present on the surface of the NiFe_2O_4 particles, diminishing significantly the complexation with AMX.

Currently, as far as the authors are aware, there are no published reports on the use of NiFe_2O_4 nanoparticles for AMX adsorption, that could be used to compare with the results presented on this article. However, the use of iron oxides in the adsorption of AMX has been reported in several papers.^{4,6,8,13,49-53} The NiFe_2O_4 nanoparticles studied presented excellent AMX adsorption results, exhibiting removal rates of 60% higher when compared to composites containing Fe oxyhydroxy supported in Al_2O_3 .¹³ This favorable ferrite performance indicates that in addition to the specific interaction of the AMX molecule with Fe, Ni should also play an important role in the adsorption of AMX. It is interesting to relate the AMX adsorption capacity of different adsorbents with their respective surface areas.

Table 5 presents some materials used in the adsorption of AMX, along with their surface areas *per* gram, and the amount of AMX adsorbed *per* surface area of the adsorbent.

In view of the results obtained, it is possible to note that NiFe_2O_4 annealed at $400 \text{ }^\circ\text{C}$ showed significantly higher adsorption capacity *per* surface area when compared with other materials reported in the literature. A possible explanation is that the main interaction of adsorbents based on activated carbon with AMX may be of van der Waals type^{54,55} whilst for composites such as Fe oxyhydroxy supported in Al_2O_3 and NiFe_2O_4 , the adsorption process is suggested to be mediated by a different interaction, being more efficient to complex AMX molecules with the

Table 5. Comparison of the adsorptive capacity of different adsorbents

Adsorbent	Surface area / (m ² g ⁻¹)	AMX adsorption / (mg m ⁻²)	Reference
Magnetically modified graphene nanoplatelets	543	0.030	49
Magnetic adsorbent prepared from olive kernel	2188	0.109	6
Mn-impregnated activated carbons	1033	0.121	53
Magnetic activated carbon with Fe ₃ O ₄	671	0.210	50
NaOH-activated carbon	2573	0.223	51
Nanoporous carbon CMK-3 type	770	0.280	52
Composites with Fe oxyhydroxy supported in Al ₂ O ₃	107	0.330	16
Nickel ferrite annealed at 300, 400, 500, 600 and 700 °C, respectively	212, 147, 53, 31 and 27	0.449, 0.600, 1.170, 1.500 and 1.670	this study

AMX: amoxicillin.

surface Fe³⁺ species, and also with Ni²⁺ species in the case of NiFe₂O₄, responsible for the higher adsorption capacity measured.

The capacity of reuse of NiFe₂O₄ in the adsorption of AMX was evaluated: in the first cycle of the experiment, the adsorbent material removed 68% of AMX, in the second cycle 59% of AMX was removed, 47% in a third cycle, and 17% removal was achieved in the fourth adsorption cycle. This satisfactory result implies a significant cost reduction in the process of using NiFe₂O₄ nanoparticles as adsorbent agent of AMX in aqueous solution.

Conclusions

NiFe₂O₄ nanoparticles were produced using the coprecipitation method, followed by thermal annealing between 300 and 700 °C, with average size between 4 and 25 nm. The adsorption capacity of NiFe₂O₄ nanoparticles to remove amoxicillin from an aqueous solution was found to depend significantly on the nanoparticle average size, the temperature, and the pH value of the solution. The adsorption process was described by a second order kinetic model and the adsorption isotherm was fitted to the Freundlich model. The amoxicillin adsorption capacity was 104, 88, 62, 46, 45 mg g⁻¹ for ferrite annealed at 300, 400, 500, 600 and 700 °C, respectively. The nanoadsorbents employed in this work showed higher amoxicillin removal efficiency than that exhibited by other iron oxides. The good reuse results obtained demonstrate that nickel ferrite nanoparticles have great potential in the removal of antibiotics by adsorption.

Supplementary Information

Supplementary data are available free of charge at <http://jbcs.sbc.org.br> as PDF file.

Acknowledgments

This work was supported by CNPq, CAPES, FAPEMIG and CNEN.

Author Contributions

Patricia M. A. Caetano was responsible for the conceptualization, data curation, investigation, resources, writing original draft, review and editing; Nathália M. Simões for the investigation and data curation; Paula S. Pinto for the conceptualization, methodology and resources; Luis E. Fernandez-Outon for the writing review and editing and visualization; Adriana S. Albuquerque for the conceptualization, project administration, resources, visualization, writing review and editing; Waldemar A. A. Macedo for the resources and visualization; José D. Ardisson for the conceptualization, data curation, formal analysis funding acquisition, project administration, resources, writing review and editing.

References

- Kümmerer, K.; *Chemosphere* **2009**, *75*, 435.
- World Health Organization (WHO); *WHO Report on Surveillance of Antibiotic Consumption: 2016-2018 Early Implementation*; WHO: Geneva, 2018. Available at http://www.who.int/medicines/areas/rational_use/oms-amr-amc-report-2016-2018/en/, accessed in June 2020.
- Chem, E. D.; Anong, D. N.; Akoachere, J. F. K. T.; *PLoS One* **2018**, *13*, e0193353.
- Hu, D.; Wang, L.; *J. Taiwan Inst. Chem. Eng.* **2016**, *64*, 227.
- Ghauch, A.; Tuqan, A.; Assi, H. A.; *Environ. Pollut.* **2009**, *157*, 1626.
- Jafari, K.; Heidari, M.; Rahmadian, O.; *Ultrason. Sonochem.* **2018**, *45*, 248.

7. Mirzaei, A.; Chen, Z.; Haghghat, F.; Yerushalmi, L.; *Chemosphere* **2017**, *174*, 665.
8. Dong, H.; Yuan, X.; Wang, W.; Qiang, Z.; *J. Environ. Manage.* **2016**, *178*, 11.
9. Koyuncu, I.; Arikan, O. A.; Wiesner, M. R.; Rice, C.; *J. Memb. Sci.* **2008**, *309*, 94.
10. Roca, M.; Villegas, L.; Kortabitarte, M. L.; Althaus, R. L.; Molina, M. P.; *J. Dairy Sci.* **2011**, *94*, 1155.
11. Zhou, J.; Wang, Y.; Wang, J.; Qiao, W.; Long, D.; Ling, L.; *J. Colloid Interface Sci.* **2016**, *462*, 200.
12. Purceno, A. D.; Teixeira, A. P. C.; de Souza, N. J.; Fernandez-Outon, L. E.; Ardisson, J. D.; Lago, R. M.; *J. Colloid Interface Sci.* **2012**, *379*, 84.
13. Pinto, P. S.; Medeiros, T. P. V.; Ardisson, J. D.; Lago, R. M.; *J. Hazard. Mater.* **2016**, *317*, 327.
14. Chayid, M. A.; Ahmed, M. J.; *J. Environ. Chem. Eng.* **2015**, *3*, 1592.
15. Gómez-Pastora, J.; Bringas, E.; Ortiz, I.; *Chem. Eng. J.* **2014**, *256*, 187.
16. Ridley, M. K.; Machesky, M. L.; Kubicki, J. D.; *Langmuir* **2015**, *31*, 703.
17. Busch, M.; Mehar, V.; Merte, L. R.; Shipilin, M.; Lundgren, E.; Weaver, J. F.; Grönbeck, H.; *Chem. Phys. Lett.* **2018**, *693*, 84.
18. Reddy, D. H. K.; Yun, Y. S.; *Coord. Chem. Rev.* **2016**, *315*, 90.
19. Weng, X.; Cai, W.; Lan, R.; Sun, Q.; Chen, Z.; *Environ. Pollut.* **2018**, *236*, 562.
20. Springer, V.; Pecini, E.; Avena, M.; *J. Environ. Chem. Eng.* **2016**, *4*, 3882.
21. Albuquerque, A. S.; Ardisson, J. D.; Macedo, W. A. A.; López, J. L.; Paniago, R.; Persiano, A. I. C.; *J. Magn. Magn. Mater.* **2001**, *226*, 1379.
22. Jia, X.; Chen, D.; Jiao, X.; He, T.; Wang, H.; Jiang, W.; *J. Phys. Chem. C* **2008**, *112*, 911.
23. Albuquerque, A. S.; Ardisson, J. D.; Macedo, W. A. A.; *J. Magn. Magn. Mater.* **1999**, *192*, 277.
24. Choi, W. O.; Lee, J. G.; Kang, B. S.; Chae, K. P.; *J. Magn.* **2014**, *151*, 38.
25. IUPAC; *Pure Appl. Chem.* **1985**, *57*, 603.
26. Caetano, P. M. A.; Albuquerque, A. S.; Fernandez-Outon, L. E.; Macedo, W. A. A.; Ardisson, J. D.; *J. Alloys Compd.* **2018**, *758*, 247.
27. Kneller, E. F.; Luborsky, F. E.; *J. Appl. Phys.* **1963**, *34*, 656.
28. Coey, J. M. D.; *Magnetism and Magnetic Materials*, 1st ed.; Cambridge University Press: Cambridge, 2010.
29. Dąbrowski, A.; *Adv. Colloid Interface Sci.* **2001**, *93*, 135.
30. Norte, T. H. O.; Marcelino, R. B. P.; Moreira, R. P. L.; Binatti, I.; Starling, M. C. V. M.; Amorim, C. C.; Pereira, E. S.; Rocha, W. R.; Lago, R. M.; *J. Environ. Eng. (U. S.)* **2018**, *144*, 04018001.
31. Anacona, J. R.; Figueroa, E. M.; *J. Coord. Chem.* **1999**, *48*, 181.
32. Anacona, J. R.; Rincones, M.; *Spectrochim. Acta, Part A* **2015**, *141*, 169.
33. Resta, R.; *Nature* **2008**, *453*, 735.
34. Hameed, B. H.; *Colloids Surf., A* **2007**, *307*, 45.
35. Fakhri, A.; Adami, S.; *J. Taiwan Inst. Chem. Eng.* **2014**, *45*, 1001.
36. Martins, A. C.; Pezoti, O.; Cazetta, A. L.; Bedin, K. C.; Yamazaki, D. A. S.; Bandoch, G. F. G.; Asefa, T.; Visentainer, J. V.; Almeida, V. C.; *Chem. Eng. J.* **2015**, *260*, 291.
37. Kaur, S. P.; Rao, R.; Nanda, S.; *Int. J. Pharm. Pharm. Sci.* **2011**, *3*, 30.
38. Hou, J. P.; Poole, J. W.; *J. Pharm. Sci.* **1971**, *43*, 445003.
39. Babić, S.; Horvat, A. J. M.; Pavlović, D. M.; Kaštelan-Macan, M.; *TrAC, Trends Anal. Chem.* **2007**, *26*, 1043.
40. Orbeci, C.; Untea, I.; Nechifor, G.; Segneanu, A. E.; Craciun, M. E.; *Sep. Purif. Technol.* **2014**, *122*, 290.
41. Sellaoui, L.; Mechi, N.; Lima, É. C.; Dotto, G. L.; Lamine, A. B.; *J. Phys. Chem. Solids* **2017**, *109*, 117.
42. Ghaznavi, F.; Fatemi, S.; Joda, M.; Weber, W. J.; Morris, J. C.; Elovich, S. Y.; Zhabrova, G. M.; Freundlich, H. M. F.; Khan, A. R.; Atallah, R.; AlHaddad, A.; Lagergren, S.; Langmuir, I.; Sips, R.; Toth, J.; *J. Chem. Phys.* **1971**, *32*, 311.
43. Ayawei, N.; Ebelegi, A. N.; Wankasi, D.; *J. Chem.* **2017**, *3039817*.
44. Dada, A. O.; Olalekan, A. P.; Olantunya, A. M.; Dada, O.; *J. Appl. Chem.* **2012**, *3*, 38.
45. Ho, Y. S.; McKay, G.; *Process Biochem.* **1999**, *34*, 451.
46. Azizian, S.; *J. Colloid Interface Sci.* **2004**, *276*, 47.
47. Khoe, G. H.; Robins, R. G.; *J. Chem. Soc., Dalton Trans.* **1988**, *8*, 2015.
48. Weng, L.; Van Riemsdijk, W. H.; Hiemstra, T.; *J. Environ. Qual.* **2012**, *41*, 628.
49. Kerkez-Kuyumcu, Ö.; Bayazit, Ş. S.; Salam, M. A.; *J. Ind. Eng. Chem.* **2016**, *36*, 198.
50. Kakavandi, B.; Esrafil, A.; Mohseni-Bandpi, A.; Jafari, A. J.; Kalantary, R. R.; *Water Sci. Technol.* **2014**, *49*, 147.
51. Pezoti, O.; Cazetta, A. L.; Bedin, K. C.; Souza, L. S.; Martins, A. C.; Silva, T. L.; Santos Jr., O. O.; Visentainer, J. V.; Almeida, V. C.; *Chem. Eng. J.* **2016**, *288*, 778.
52. Barrera, D.; Villarroel-Rocha, J.; Tara, J. C.; Basaldella, E. I.; Sapag, K.; *Adsorption* **2014**, *20*, 967.
53. Liu, H.; Hu, Z.; Liu, H.; Xie, H.; Lu, S.; Wang, Q.; Zhang, J.; *RSC Adv.* **2016**, *6*, 11454.
54. Li, Y.; Zhang, J.; Liu, H.; *Water* **2018**, *10*, 351.
55. Jalil, M. E. R.; Baschini, M.; Sapag, K.; *Materials* **2017**, *10*, 1345.

Submitted: February 27, 2020
Published online: June 19, 2020

